Journal of Applied Electrochemistry **30**: 551–559, 2000.

Steady-state operation of a compressor for a proton exchange membrane fuel cell system

D. THIRUMALAI and R.E. WHITE*
Department of Chemical Engineering, University of South Carolina, Columbia, SC 29208, USA
*(*author for correspondence)*

Received 6 August 1998; accepted in revised form 23 February 1999

Key words: compressor, fuel cell, system operation

Abstract

The performance of a system consisting of a proton exchange membrane (PEM) fuel cell coupled to a centrifugal air compressor is simulated. Two modes of operation of the system are investigated: one in which the speed of the compressor is constant, and the other in which the compressor speed is varied with the electric load on the fuel cell stack. The operating characteristics of the compressor and the PEM fuel cell stack and their influence on the system efficiency are analyzed for a step change in the stack current. The effects of the fuel cell stack back-pressure and the electric load on the compressor power consumption and the system efficiency are studied. It is found that the system efficiency is higher when the fuel cell stack is operated at a constant oxygen gas stoichiometry by varying the compressor speed instead of at a constant compressor speed. The system model can be used to determine the rotation speed of the compressor for various electric loads.

List of symbols

A_{cell}	active area per cell (cm^2)
$C^*_{O_2}$	gas phase concentration of oxygen (mol cm^{-3})
E_{oc}	open-circuit voltage of a single fuel cell (V)
F	Faraday's constant (96 500 A s mol^{-1})
H	fraction of the compressor's design head
H_{ad}	adiabatic head developed by the compressor (m)
i	operating current density (A cm^{-2})
I_{FC}	current drawn from the fuel cell system (A)
$m^{in}_{O_2}$, $m^{out}_{O_2}$	inlet and outlet flowrates of oxygen gas (mol s^{-1})
N	fraction of the compressor's design rotation speed
N_{comp}	rated compressor rotation speed, assumed to be 5000 rpm
N_{cell}	number cells in a fuel cell stack
$p^*_{H_2}$	average partial pressure of oxygen (atm)
$p^*_{O_2}$	average partial pressure of hydrogen (atm)
P	average stack operating pressure (kPa)
P_{back}	pressure at the stack outlet (kPa)
P_1, P_2	gas pressure at compressor inlet and discharge, respectively (kPa)
P^w_{sat}	vapour pressure of water at the operating temperature (kPa)
P_{comp}	power consumed by the compressor (kW)
P_{FC}	power generated by the fuel cell (kW)
Q	fraction of the compressor's design inlet gas flowrate
Q_1	gas flowrate at the compressor inlet (m^3 h^{-1})
Q_{STK}	gas flowrate at the fuel cell stack inlet (m^3 h^{-1})
R	gas constant (J $kmol^{-1}$ K^{-1})
S_{O_2}	oxygen stoichiometry
T_a	ambient temperature (assumed 293.15 K)
T_1	compressor inlet temperature (assumed to be equal to T_a)
T	operating temperature (K)
V	cell voltage (V)
$x^{avg}_{N_2}$	average mole fraction of nitrogen
$x^{in}_{N_2}$	mole fraction of nitrogen in the inlet gas
ΔP_{STK}	pressure drop across the stack (kPa)

Greek symbols

γ	ratio of specific heats of a gas, assumed 1.4 for air
η_{act}	activation overvoltage (V)
η_{ohm}	voltage drop due to membrane resistance (V)

η_N	compressor operating efficiency
$\eta_{N=100\%}$	compressor efficiency at the rated rotation speed
η_{sys}	PEM fuel cell/compressor system efficiency

Parameters

A–D, α, β	compressor head-flowrate relationship (dimensionless)
E, F, G	efficiency of the compressor at the rated speed (dimensionless)
H_j, $Q_j (j = L, R)$	isoefficiency lines of the compressor (dimensionless)
K_1, K_2	constants characterizing an isoefficiency line that are calculated as part of the solution procedure (dimensionless)
k_{FF}	resistance of the flow field for gas flow (kPa m^{-3} h)
k_{MN}	resistance of the stack manifold for gas flow (kPa m^{-6} h^2)
ξ_1–ξ_7	parameters that describe fuel cell voltage dependance on operating conditions (refer to Table 3 for units)

1. Introduction

Fuel cell powered vehicles have the environmental benefits inherent in electric vehicles without the disadvantages of long charging times and limited range associated with battery powered vehicles. There is tremendous interest in the commercialization of PEM fuel cell based power systems for automobile and stationary applications because of the PEM fuel cell's high operating current density, efficiency and fast start-up time.

Various mechanistic and empirical models of fuel cells are available in the literature [1–6]. The emphasis of all the above models is on the performance of single fuel cells operating in isolation. In practice, PEM fuel cells are connected to auxiliaries like compressors, humidifiers etc. The major parasitic power loss in a PEM fuel cell system is due to the compressor used to deliver air. A detailed understanding of the influence of the compressor on the PEM fuel cell operation is essential for system optimization and control. These issues have not received wide exposure in the available literature since fabrication of large-scale fuel cell power systems is a recent development. This study focuses on the coupling of the fuel cell stack performance to the operation of the air compressor.

In this study a continuous stream of pure hydrogen at the desired operating pressure is assumed to be available (compressed gas) and is used as the fuel. Ambient air delivered to the fuel cell via a compressor is the cathode reactant. Operation at higher air pressures typically results in higher fuel cell performance [1]. The performance of the fuel cell is strongly dependent on the oxygen concentration at the catalyst surface. The oxygen stoichiometry is defined as

$$S_{O_2} = \frac{m_{O_2}^{in}}{m_{O_2}^{in} - m_{O_2}^{out}} \tag{1}$$

where $m_{O_2}^{in}$ and $m_{O_2}^{out}$ are the inlet and outlet molar flowrates of oxygen gas.

Hence, for a specific operating current density, higher inlet air flowrate, which implies higher oxygen gas stoichiometry, increases the effective concentration of oxygen with the resultant increase in the fuel cell performance. This increase in the fuel cell performance at higher operating pressures and air flowrates comes at the cost of increasing power consumption by the compressor. Various compressor control strategies are analysed and a quantitative measure of the system efficiency is obtained for different modes of operation.

A schematic of a PEM fuel cell system with an air compressor is given in Figure 1. A back-pressure regulator at the air outlet controls the operating pressure on the air side. The rotation speed of the compressor motor controls the inlet air flowrate and the pressure rise across the compressor. The gas manifolds of the fuel cell stacks are connected in parallel and a compressor is used to deliver air to all the fuel cell stacks. In this study an internally humidified stack that contains a humidification section integral to the stack is used [7].

The design parameters and rated operating conditions for the system under consideration are given in Table 1.

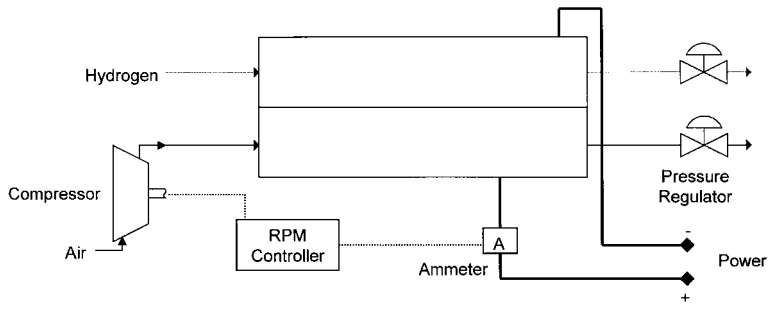

Fig. 1. PEM fuel cell with an air compressor.

Table 1. System design parameters used in the analysis

Power system	252 kW
2 parallel trains each with 10 stacks connected electrically in series.	
360 A current in each of the trains, total current of $(0.4 \times 900 \times 2)$ 720 A.	
Bus voltage at design operating conditions is about $(0.7 \times 50 \times 10)$ 350 V.	
Fuel cell stack	
Number of cells, N_{cell}	50
Active area per cell, A_{cell}	900 cm^2 (30 cm × 30 cm)
Anode reactant	Pure compressed hydrogen
Cathode reactant	Saturated air
Operating conditions (design)	
Pressure, P_{back}	303.9 kPa
Operating temperature, T	353.15 K
Ambient temperature, T_a	293.15 K
Current density, i	0.4 A cm^{-2}
Cell voltage, V	0.7 V
Oxygen stoichiometry, S_{O2}	2.0
Compressor rating	
Inlet gas flowrate, Q_1	770 m^3 h^{-1}
Rotation speed	5000 rpm
Compression ratio, P_2/P_1	3.0

The fuel cell power system is assumed to consist of two parallel trains of fuel cell stacks with 10 stacks connected in series in each train as shown in Figure 2. The fuel cell stack used in the analysis is assumed to be designed for operation at about 303.9 kPa back-pressure (P_{back}), 80 °C temperature (T) and 0.4 A cm^{-2} current density (i), with an active area (A_{cell}) of 900 cm^2 per cell). For fixing the design, the fuel cell is assumed to generate 0.7 V per cell under these conditions. The above operating conditions are fixed such that the fuel cell operates close to the operating regime of the Ballard Mark IV fuel cells [8], one of the few fuel cells that have been used to build large PEM fuel cell stacks. Thus the fuel cell system is designed to deliver a total current of 720 A with a bus voltage of about 350 V, about 252 kW.

Typical use of the fuel cell powered vehicle with its varying power demand necessitates the use of some form of control for energy efficient operation. Different modes of operation of the fuel cell system are discussed in a recent work [9] and are summarized below:

(i) Operation of the compressor at constant speed.
(ii) Varying the compressor speed such that a constant oxygen stoichiometry is maintained at all power levels.
(iii) Varying both the compressor speed and the operating pressure to reduce the parasitic power loss at the compressor.

The operation of the compressor–PEM fuel cell system was studied previously [9] with consideration to the performance model of only the fuel cell. The efficiency of the compressor was assumed to be constant. This is an extension of the above work in that the model of a centrifugal compressor is coupled to that of the fuel cell and the system performance is studied. Also, the change in rotation speed of the compressor required for a specified change in the current drawn from the fuel cell can be predicted using the system model presented here. Quantitative measures of the system efficiency for the different modes of operation are presented.

2. Compressor characteristics

The performance of a centrifugal compressor is characterized by the head developed by the compressor at each inlet gas flowrate at different rotation speeds of the impeller. Also, compressor efficiency data is specified as isoefficiency lines that are overlaid on the compressor characteristic curves. The modeling of compressor systems is discussed with varying levels of detail in the literature [10–13] and requires user supplied tables of efficiency and head-flow data at various rotation speeds.

For this study empirical equations and the algorithm to map compressor data were chosen from the literature [13]. The fraction of the rated head developed by centrifugal compressors of similar design is given by

$$H = AN^2 + BNQ + CQ^2 + D(1 - N^\alpha)Q^\beta \quad (2)$$

where N is the fraction of the rated rotational speed, Q is the fraction of the rated inlet gas flowrate and the other

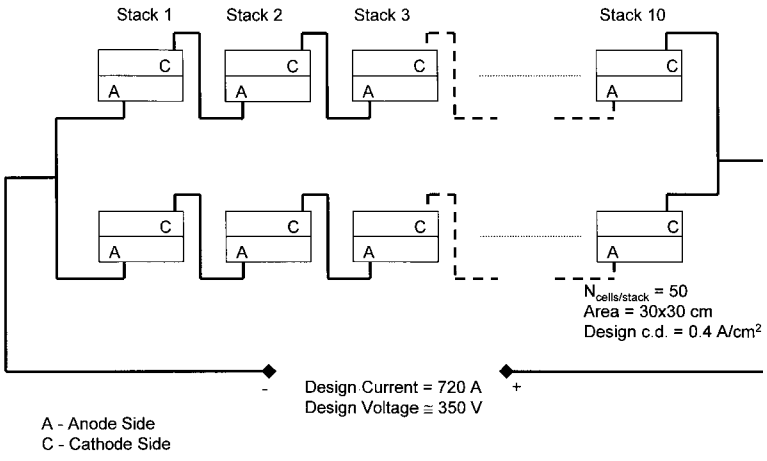

Fig. 2. Electrical schematic of the power system analysed.

variables are model parameters. The compressor efficiency at the rated rotational speed is given by

$$\eta_{N=100\%} = E + FQ^2 + GQ^4 \tag{3}$$

where E, F and G are fitted parameters. The isoefficiency lines to the left and right of the maximum efficiency line (Fig. 3) are as follows:

$$\text{Right: } H - H_R = K_1(Q + Q_R)^2 \tag{4a}$$

$$\text{Left: } H - H_L = K_2(Q + Q_L)^{0.5} \tag{4b}$$

The parameters are obtained by fitting the equations to the representative compressor data from the literature [13] using the Powell hybrid method [14].

The model parameters are given in Table 2 and the fit to the data is in Figure 3. It is seen that the compressor head decreases with increasing flow for most part of the operating region. At each rotation speed, as the flow is reduced below a certain value, the head developed by the compressor begins to fall. This leads to a well-known phenomenon called surge that produces unstable operation due to momentary reversal of flow in the compressor. The compressor should not be operated in this region and most compressor systems are equipped with surge protection systems.

The efficiency at the rated speed is given in Figure 4. If the operation is away from the rated flow as may occur in fuel cell systems during periods of peak or low power demands, the efficiency of the compressor suffers. The operating pressure can be changed to accommodate the flow requirement. But this may lead to undesirable conditions since the gas in the channels and manifold is saturated with water vapour that may condense and disrupt the flow patterns. An optimal solution to this problem is to vary the rotation speed of the compressor, thus explicitly controlling the operating point, that is, the pressure and the gas flowrate. The above equations, in conjunction with the equation describing the hydraulic behaviour of the stack, discussed in the following Section, are solved using the Newton–Raphson method to obtain the efficiency and rotation speed of the compressor for a specified operating pressure and gas inlet flowrate.

Table 2. Parameters for the empirical equations describing the compressor performance obtained by fitting the equations to compressor characteristics data (Fig. 2) from the literature [13]

Dimensionless parameters in Equation 2	
A	0.510
B	1.581
C	−1.090
D	−20.011
α	0.015
β	3.046
Dimensionless parameters in Equation 3	
E	0.623
F	0.433
G	−0.265
Dimensionless parameters in Equations 4(a) and (b)	
H_L	−8.653
Q_L	1.837
H_R	−1.131
Q_R	2.790

The power consumption, P_{comp}, and the adiabatic head, H_{ad}, developed by the compressor are given in [15] as follows:

$$P_{comp} = \frac{1}{\eta_N} 2.78 \times 10^{-4} \frac{\gamma}{\gamma - 1} Q_1 P_1 \left[\left(\frac{P_2}{P_1} \right)^{\gamma - 1/\gamma} - 1 \right] \tag{5}$$

$$H_{ad} = \left(\frac{\gamma}{\gamma - 1} \right) \times \frac{RT_1}{9.806 \times 28.84} \left[\left(\frac{P_2}{P_1} \right)^{\gamma - 1/\gamma} - 1 \right] \tag{6}$$

where η_N is the operating efficiency, Q_1 is the inlet gas flowrate, T_1 is the inlet temperature, P_1 and P_2 are inlet and discharge pressures, respectively, and γ is the ratio of specific heats (1.4 for a diatomic gas).

3. Fuel cell performance model

3.1. *Gas flow behaviour*

The principal resistance to gas flow in fuel cell stacks is due to the flow fields that distribute the reactant gas

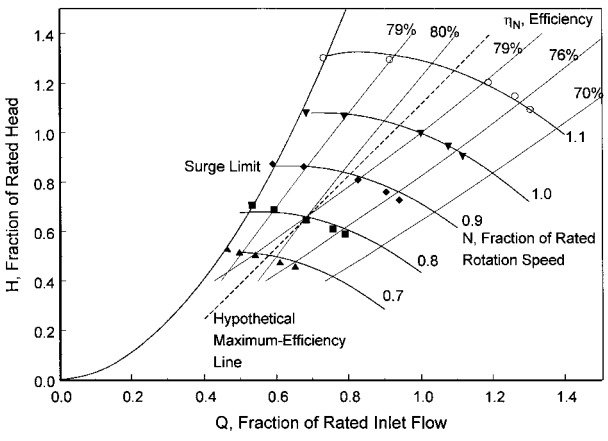

Fig. 3. Typical compressor characteristics.

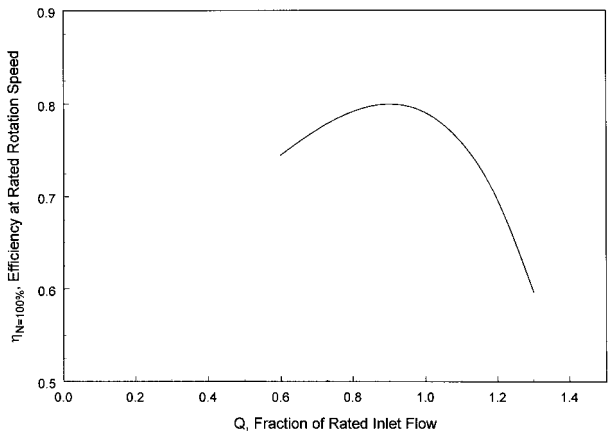

Fig. 4. Compressor efficiency at rated rotation speed.

across active surface area of the gas diffuser and membrane electrode assembly (MEA). Flow fields can be in the form of a block of porous material that is in contact with the gas diffuser and the pressure drop across it is given by Darcy's law [16]. Another type is the interdigitated flow field, where the gas flow is through the thin gas diffuser backing. This may lead to potentially better fuel cell performance [17], but the pressure drop may be high. Graphite or carbon composite plates with grooves for gas flow are extensively used in commercial fuel cell stacks [18]. The dependance of the pressure drop on the gas flowrate is related to the geometry of the individual channel and also the design patterns that the grooves form on the carbon plate. This study assumes the use of the above ribbed flow fields.

Data on the pressure drop-flow relationship for these flow fields are not available in the open literature to the authors' knowledge. Previous work on the modeling of flow fields with a rectilinear network of grooves predicted a linear relationship between the pressure drop and the gas flowrate [19]. The present work models the pressure drop (in kPa) across the stack as a sum of the contributions due to the flow of gas in the flow field and the gas manifold. The pressure drop in the manifold is assumed to be smaller than that in the flow field and is given as follows by the empirical equation:

$$\Delta P_{\mathrm{STK}} = k_{\mathrm{FF}} \frac{Q_{\mathrm{STK}}}{N_{\mathrm{cell}}} + k_{\mathrm{MN}} Q_{\mathrm{STK}}^2 \tag{7}$$

k_{FF} and k_{MN} are parameters that depend on the flow field design, the gas flow configuration, stack design, fittings etc. In this study the values of k_{FF} and k_{MN} are arbitrarily selected to be 30.33 kPa m^{-3} h and 0.0 kPa m^{-6} h^2, respectively. Q_{STK} is the gas flowrate at the inlet of a single stack. Since all the stacks are connected in parallel with respect to the air and hydrogen gas flow, Q_{STK} is related to the inlet flow at the compressor and is given below:

$$Q_{\mathrm{STK}} = \frac{1}{20} Q_1 \frac{101.3}{(P_2 + P_{\mathrm{back}})/2} \left(\frac{T}{T_{\mathrm{a}}}\right) \tag{8}$$

where T_{a} and T are the ambient and operating temperature, respectively. The discharge pressure of the compressor is given by

$$P_2 = \Delta P_{\mathrm{STK}} + P_{\mathrm{back}} \tag{9}$$

where P_{back} is the back pressure set by the operator.

3.2. *Electrochemical performance*

The empirical model of the Ballard Mark IV fuel cell is used to describe the current voltage relation since the fuel cell modelled has been used to build large stacks that are of interest in this study. The cell voltage, V, is the sum of the open circuit potential, E_{oc}, the activation overvoltage, η_{act}, and the ohmic drop in the membrane, η_{ohm}, and is given below (from [6]):

$$\begin{aligned} V &= E_{\mathrm{oc}} + \eta_{\mathrm{act}} + \eta_{\mathrm{ohm}} \\ E_{\mathrm{oc}} &= 1.229 - 0.85 \times 10^{-3}(T - 298.15) \\ &\quad + 4.3085 \times 10^{-5}\, T\left[\ln(p^*_{\mathrm{H}_2}) + \tfrac{1}{2}\ln(p^*_{\mathrm{O}_2})\right] \\ \eta_{\mathrm{act}} &= \xi_1 + \xi_2 T + \xi_3 T \ln(C^*_{\mathrm{O}_2}) + \xi_4 T \ln(50.56\, i) \\ \eta_{\mathrm{ohm}} &= -i(\xi_5 + \xi_6 T + \xi_7 i) \end{aligned} \tag{10}$$

where T is the operating temperature, i the cell current. $C^*_{\mathrm{O}_2}$ is the concentration of oxygen at the interface. The parameters, ξ_i, used here are similar to those in reference [6] and are summarized in Table 3.

The interface concentration of oxygen, $C^*_{\mathrm{O}_2}$, is given as follows [8]:

$$C^*_{\mathrm{O}_2} = \left(\frac{1}{101.3}\right)\left[\frac{P - P^{\mathrm{w}}_{\mathrm{sat}} - P x^{\mathrm{avg}}_{\mathrm{N}_2} \exp\left(\frac{0.291\, i}{T^{0.852}}\right)}{5.08 \times 10^6 \exp\left(\frac{-498}{T}\right)}\right] \tag{11}$$

where $P^{\mathrm{w}}_{\mathrm{sat}}$ is the vapour pressure of water at the operating temperature. The operating pressure of the stack, P, is the average of the inlet and outlet pressures and is $(P_2 + P_{\mathrm{back}})/2$.

Assuming both the inlet and outlet cathode gas streams to be saturated, the mole fraction of N_2 in the cathode outlet gas stream is 0.79 $\left(P_{\mathrm{back}} - P^{\mathrm{w}}_{\mathrm{sat}}\right)/P_{\mathrm{back}} \times S_{\mathrm{O}_2}/(S_{\mathrm{O}_2} - 0.21)$ using the definition of stoichiometry (Equation 1). The current efficiency of oxygen reduction is assumed to be 100% (transport of gaseous oxygen across the membrane is negligible). Hence, the average mole fraction of nitrogen, $x^{\mathrm{avg}}_{\mathrm{N}_2}$, is related to the stoichiometry of oxygen and is as follows:

$$x^{\mathrm{avg}}_{\mathrm{N}_2} = \frac{1}{2}\left[x^{\mathrm{in}}_{\mathrm{N}_2} + \left(0.79 \times \frac{P_{\mathrm{back}} - P^{\mathrm{w}}_{\mathrm{sat}}}{P_{\mathrm{back}}} \times \frac{S_{\mathrm{O}_2}}{S_{\mathrm{O}_2} - 0.21}\right)\right] \tag{12}$$

The oxygen stoichiometry and the actual inlet air flowrate at the compressor are related to the current drawn from the fuel cell system, I_{FC} by Faraday's law and is given below after consideration to the electrical circuit and the ambient temperature.

$$Q_1 = (20\, N_{\mathrm{cell}}) 80.64 \times \frac{T_{\mathrm{a}}}{273.15} \times \frac{S_{\mathrm{O}_2}}{0.21} \times \frac{I_{\mathrm{FC}}/2}{4F} \tag{13}$$

where F is the Faraday's constant and T_{a} is the ambient temperature, assumed to be 293.15 K in this study.

Table 3. Parameters for the fuel cell performance equations used in this study

ξ_1	−0.9514 V
ξ_2	0.00312 V K^{-1}
ξ_3	7.4×10^{-5} V K^{-1}, $C^*_{\mathrm{O}_2}$ in mol cm^{-3}
ξ_4	1.87×10^{-4} V K^{-1}, i in A cm^{-2}
ξ_5	0.8115 Ω
ξ_6	-1.77×10^{-3} Ω cm^2 K^{-1}
ξ_7	0.205 Ω cm^4 A^{-1}
k_{MN}	0 kPa m^{-6} h^2
k_{FF}	30.33 kPa m^{-3} h

The power generated by the fuel cell system is given by

$$P_{FC} = \frac{1}{10^3}(10.50)V\ I_{FC} \tag{14}$$

where I_{FC} is the current drawn from the fuel cell.

The ratio of the net power output by the compressor-fuel cell system to the gross power generated by the fuel cell stack is defined as the system efficiency and is given below.

$$\eta_{sys} = \frac{P_{FC} - P_{comp}}{P_{FC}} \tag{15}$$

where P_{FC} is the power generated by the fuel cell and P_{comp} is the power consumed by the compressor. The system efficiency as defined above is equivalent to the mechanical efficiency as used in internal combustion engine study.

4. Results and discussion

The pressure drop-flowrate relationship curve is overlaid on the compressor characteristics in Figure 5. Each intersection of the fuel cell system curve with a compressor characteristic curve defines a unique operating point. It can be seen that the compressor rotation speed offers a degree of freedom that can be used to fix the operating point at a specified inlet gas flowrate for any particular back-pressure, P_{back}.

The compressor power consumption over a range of gas flowrates at different back-pressures is given in Figure 6. At gas flow rates higher than the rated flow, 770 $m^3\ h^{-1}$, the effect of back pressure on the compressor power consumption is lower. Also, as expected, the power consumption decreases with decrease in the gas flowrate and operating pressures.

A 30% drop (step change down) in the operating current is imposed on the system as shown in Figure 7(a) and the system performance is analysed.

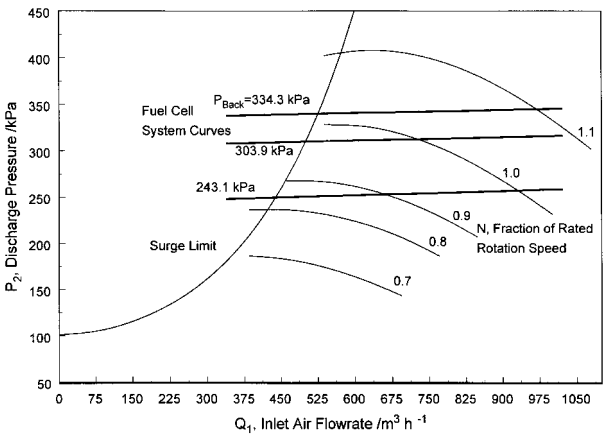

Fig. 5. System operating curves. Each operating point is uniquely determined by the intersection of the system curve with the compressor characteristics.

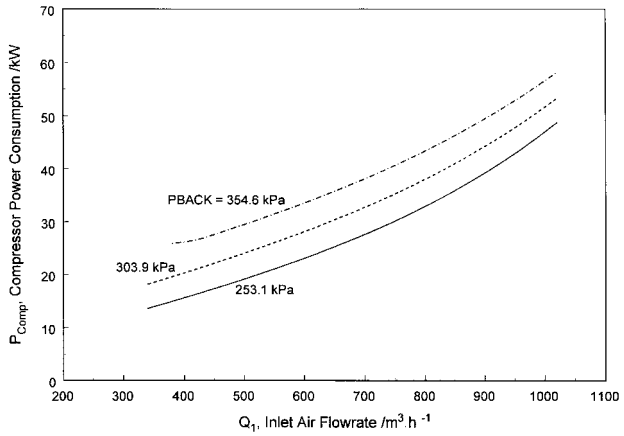

Fig. 6. Effect of gas flowrate and operating pressure on the compressor power consumption.

The abscissae in Figures 7–9 are hypothetical since transients are not considered in this study. The numerical values in the abscissa are given only as a reasonable estimate of time over which the study is applicable. The solution methodology for calculation of various measures of performance of the system, N, P_{FC}, P_{comp}, and η_{sys}, is illustrated by calculating them for specific operating regions.

4.1. *Compressor rotation speed for maintaining constant S_{O_2} (Figure 7(b))*

This Section deals with the calculation of the required compressor speed to maintain a constant S_{O_2} when the current drawn from the fuel cell system is changed. At constant oxygen stoichiometry, the required inlet air flowrate at the compressor is calculated using Equation 13 and the discharge pressure at the compressor is calculated using Equations 7–9. The required change in compressor speed is then calculated by solving the Equation 2. The specific case of the reduction in the current drawn from the fuel cell system (operating at the design conditions as given in Table 1) from 720 to 504 A (Fig. 7(b)) is discussed next.

For the case of operation at a constant stoichiometry, $S_{O_2} = 2.0$, the required inlet gas flowrate is calculated from Equation 13 as 538.1 $m^3\ h^{-1}$. Thus the fraction of rated inlet flowrate (rated flowrate is 770 $m^3\ h^{-1}$), Q, is 0.7. The discharge pressure, P_2, calculated by solving Equations 7–9 by using Newton–Raphson method is found to be 310.4 kPa. The compressor head, H_{ad}, corresponding to this discharge pressure calculated from Equation 6 is 1.14×10^4 m. The compressor rated head is obtained by substituting the design compression ratio, $P_2/P_1 = 3$, in Equation 6 and is found to be 1.11×10^4 m. Thus the fraction of rated head, H, at the specific operating condition is 1.022. Equation 2 is solved with these calculated values of Q and H to obtain N, the fraction of rated rotation speed as 0.97.

Thus the compressor speed is reduced from 5050 rpm (for operation at 720 A) to 4850 rpm to maintain constant stoichiometry of 2.0 as seen in Figure 7(b).

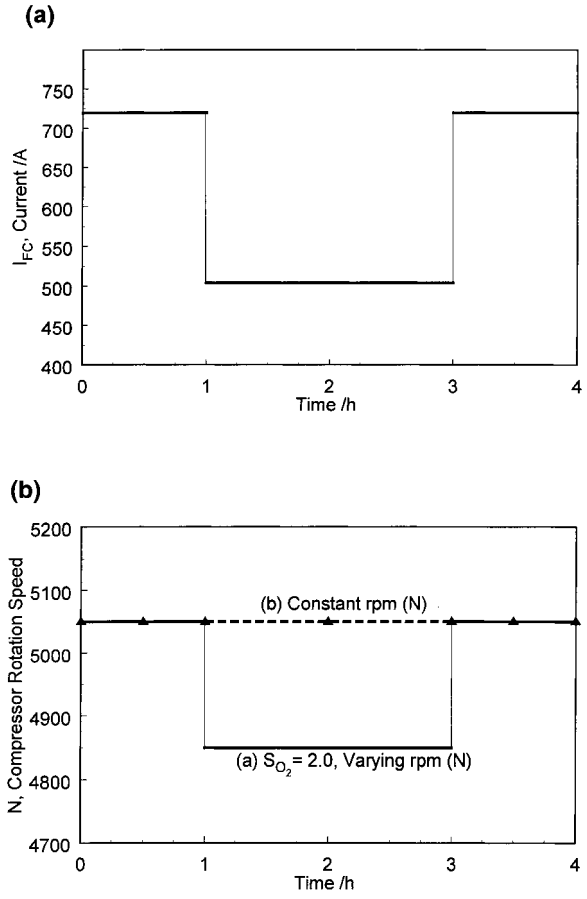

Fig. 7. (a) Step change in the current drawn from the system. (b) Variation in the compressor speed required to maintain (*a*) constant oxygen stoichiometry, varying rpm, (*b*) constant rpm.

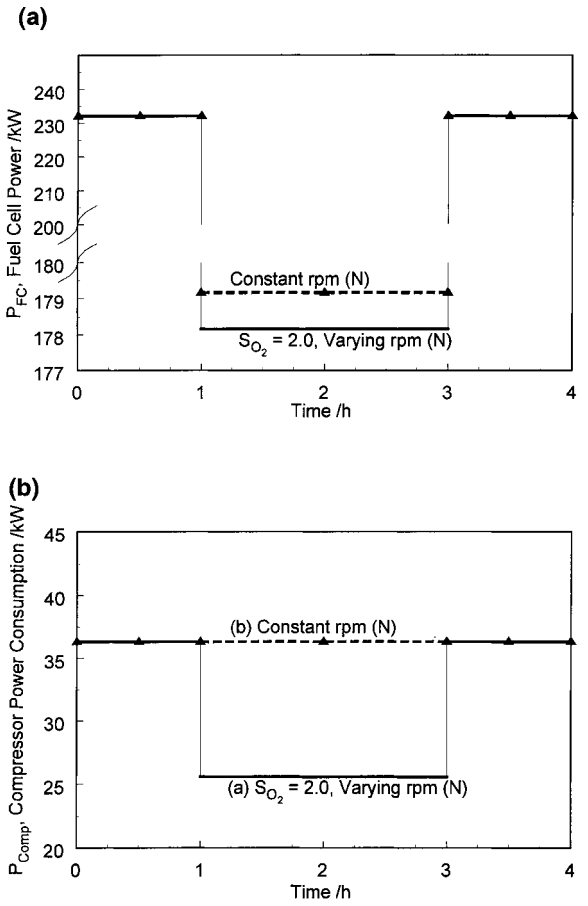

Fig. 8. (a) Changes in the fuel cell performance for the constant rpm and constant stoichiometry cases. Constant rpm case results in marginally higher fuel cell performance. (b) Changes in the compressor power consumption. The constant rpm (case b) results in higher power consumption.

4.2. *Power generated by the fuel cell (Figure 8(a))*

The solution procedure to calculate the cell voltage and the power generated by the fuel cell is discussed. At constant compressor rotation speed, the inlet air flowrate is constant. Hence, the oxygen stoichiometry varies with the current drawn from the system and is calculated from Equation 13. When a variable speed drive is used with the compressor, the stoichiometry can be maintained at the desired value as discussed in Section 1. For both cases, the cell voltage is obtained using Equations 10–12 and the power generated by the fuel cell system is calculated from Equation 14. Specific cases are discussed below to illustrate the procedure.

For the constant rpm case, the inlet flowrate, Q_1, is constant at 768.8 $m^3\ h^{-1}$ (flowrate calculated for operation at 720 A, from Equation 13) and hence, the oxygen stoichiometry, S_{O_2}, increases from 2.0 to 2.9 (calculated from Equation 13) for the drop in current from 720 to 504 A. The nitrogen mole fraction in the inlet gas, $x^{in}_{N_2}$, is 0.671 (for saturated air at temperature, T, 353.15 K and pressure (calculated as in Section 1), P_2, 313.2 kPa). The average nitrogen mole fraction obtained from Equation 12 is 0.696. The concentration of oxygen at the interface, $C^*_{O_2}$, calculated from Equation 11 is 0.371×10^{-6} mol cm^{-3} (the average pressure, P, is 308.6 kPa and the vapor pressure of water, P^w_{sat}, is 47.2 kPa at 353.15 K). The operating current density is given by $i = I_{FC}/2900 = 0.28$ A cm^{-2}, for this case. For saturated pure hydrogen gas at the same temperature and pressure as the cathode gas, the partial pressure of hydrogen, $p^*_{H_2}$, is 2.6 atm (310.4–47.2 kPa). The partial pressure of oxygen at the interface, $p^*_{O_2}$, is given by [8]

$$p^*_{O_2} = \frac{1}{101.3}\left(P - P^w_{sat} - Px^{avg}_{N_2}\exp\left(\frac{0.291i}{T^{0.832}}\right)\right) = 0.46 \text{ atm} \quad (16)$$

These values are substituted in Equation 10 to obtain the cell voltage, V, as 0.711 V. The open circuit voltage, E_{oc}, is 1.191 V and the activation overpotential (η_{act}) and the ohmic drop (η_{ohm}) are −0.412 V and −0.068 V, respectively. Similar calculations for other conditions are performed.

The cell voltage increases from 0.645 V (for 720 A current) to 0.711 V in the above case. Thus, the power generated in this case calculated from Equation 14 is 179.2 kW. When the compressor speed is varied and the stoichiometry, S_{O_2}, is maintained at 2.0, the cell voltage increases to 0.707 V from an initial value of 0.645 V.

The change in the fuel cell voltage and hence the power delivered is given in Figure 8(a). It is seen that the fuel cell power produced by operation at constant compressor speed is marginally higher than in the case where the stoichiometry is constant.

4.3. *Compressor power consumption (Figure 8(b))*

The calculation of the compressor efficiency and the power consumption by the compressor is presented here. The head developed by the compressor at the operating point (characterized by Q_1 and P_2) is calculated from Equation 6. It is then determined whether the operating point falls to the left or right of the maximum efficiency line. The constant, K_1 or K_2, in the equation for the appropriate isoefficiency line (Equation 4(a) or 4(b)) that passes through the operating point is determined. The intersection of the isoefficiency line with the compressor characteristic at the rated rotation speed ($N = 1.0$) is calculated by solving Equations (4(a) or 4(b)) and Equation 2. The flowrate, $Q_{N=100\%}$, corresponding to this point is substituted in Equation 3 to obtain the compressor efficiency. The power consumption by the compressor is determined from Equation 5. The system efficiency is calculated using Equation 15 for all the cases. To illustrate the above procedure, the compressor power consumption at the design operating point, 720 A current load at a stoichiometry (S_{O_2}) of 2.0, is calculated.

The procedure for finding the operating conditions, (Q, H), are the same as that discussed in the calculation of the compressor speed, Q, and were found to be 0.998, and 1.032, respectively. The flowrate, Q, that maximizes the efficiency at the rated speed, $N = 1.0$, is given by

$$\frac{d\eta_{N=100\%}}{dQ} = F2Q + G4Q^3 = 0 \tag{17}$$

Hence,

$$Q = \left(-\frac{F}{2G}\right)^{1/2} \tag{18}$$

The Q calculated above ($Q = (E/2G)^{1/2}$) and the corresponding fractional head, H, calculated from Equation 2 (with $N = 1.0$), are given by 0.904, 1.048. Assuming the equation of the maximum efficiency line is of the form Equation 4(b), the value of K_2 for this line is 5.86, obtained by substituting the above values of Q and H in Equation 4(b). The fractional head, H, corresponding to the point on the maximum efficiency line at the operating flowrate, $Q = 0.998$, is obtained by substituting this value of Q in Equation 4(b). It is given by

$$H = H_L + 5.86\,(0.998 + Q_L)^{1/2} = 1.214 \tag{19}$$

Since the head corresponding to the operating point, $H = 1.032$, is less than the above calculated value of 1.214, the operating point lies to the right of the maximum efficiency line (Figure 3) and Equation 4(a) applies to the isoefficiency line passing through the operating point (0.998, 1.032). The value of K_1 for this line is given by

$$K_1 = \frac{1.032 - H_R}{(0.998 + Q_R)^2} = 0.151 \tag{20}$$

Solving the equation for this isoefficiency line, Equation 4(a) with $K_1 = 0.151$, and Equation 2, with N set to 1.0, gives the point corresponding to the intersection of the design head-flowrate curve and the isoefficiency line passing through the operating point. It is found to be (0.981, 1.012). Substituting this value of Q, 0.981, in Equation 3 gives the efficiency of the operating point, η_N, and is found to be 0.794. The compressor power consumption, P_{comp}, found from Equation 5, is 36.3 kW ($Q_1 = 768.8\ m^3\ h^{-1}$ and $P_2 = 313.2$ kPa, calculated as in Section 1). The system efficiency, η_{sys}, at this operating point is obtained from Equation 15 as 0.844 (the fuel cell power, P_{FC}, is 232.2 kW, calculated as in Section 2).

The compressor power consumption for both cases, constant rotation speed and constant stoichiometry, are given in Figure 8(b). The power consumed is significantly reduced in the case of constant stoichiometry but remains the same for operation at constant rotation speed.

4.4. *Efficiency of operation (Figure 9)*

It is seen from Figure 9 that the system efficiency, defined in Equation 15, is higher after the step change in the case of constant stoichiometry due to the decreased gas throughput in the compressor. A significant decrease in system efficiency is observed for the case of operation at constant compressor speed.

It is to be noted that the model is steady state and the transient changes in the cell voltage near the step change are not modelled. The time constant of these transients is of the order of 0.002 to 0.01 s [20] and is not relevant in the time scale considered here. Changes in membrane

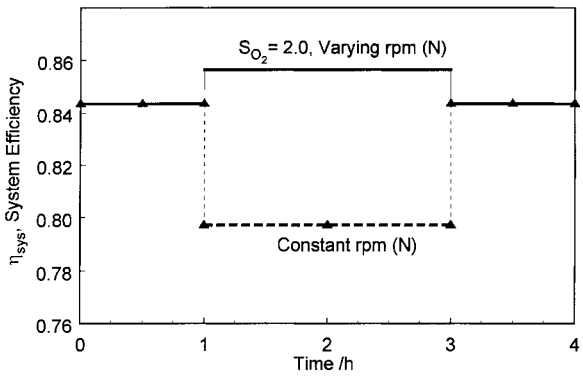

Fig. 9. The constant stoichiometry, S_{O_2}, mode operates at higher efficiencies at lower currents in contract to the much lower efficiencies exhibited by the constant speed, N, mode.

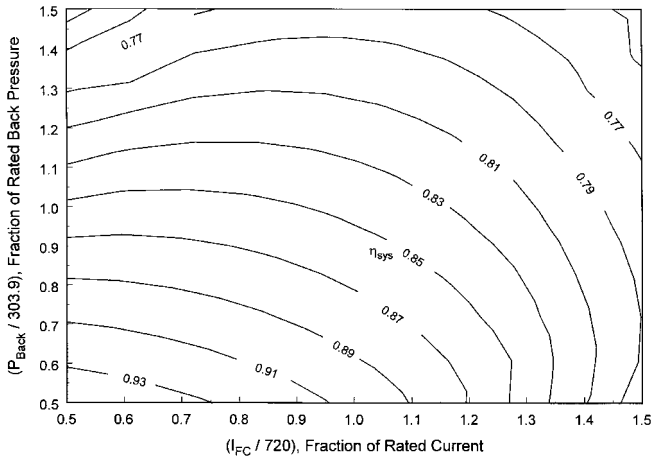

Fig. 10. Variation of the system efficiency with the current load and the operating pressure. Rated current, $I_{FC} = 720$ A (0.4 A cm^{-2}); rated back pressure, $P_{back} = 303.9$ kPa.

hydration states and variations in the temperature due to the slow dynamics of the coolant loop introduce transients with larger time constants, but these effects are outside the scope of this study.

To evaluate the case of decreasing the operating pressure in addition to maintaining a constant stoichiometry (case c) the change in the system efficiency at different operating pressures and currents (with the stoichiometry set to 2.0) are plotted in Figure 10. From the contour plot, it is seen that for operation to the right of the rated current (greater then 1.0) any control action involving a decrease in pressure does not contribute to any increase in efficiency. In contrast a decrease in pressure marginally improves the system efficiency for operation to the left of the rated current. Further sudden swings in the operating pressure are not conducive to stable operation of the system. Thus the control strategy of maintaining a constant stoichiometry (case b) by varying the compressor speed is optimal from a power efficiency point of view.

5. Conclusions

The operation of the compressor fuel cell system is analyzed at different operating conditions. A method to obtain the speed of the compressor for a specific operating condition is developed. This strategy could be implemented using microcontrollers for scheduling the compressor speed. Compressor operation at constant speed is the most inefficient form of operation. It is found that the marginally better performance of the fuel cell at higher stoichiometry (as in the case for constant rpm at reduced current load) is offset by the higher power consumption by the compressor thus reducing the overall efficiency. The strategy of varying the compressor speed to maintain a constant oxygen stoichiometry leads to efficient operation over a wide range of power demands.

Acknowledgements

The authors are grateful for the support of this work by the DOE/EPSCoR program.

References

1. J. Kim, S.M. Lee, S. Srinivasan and C.E. Chamberlain, *J. Electrochem. Soc.* **142** (1995) 2670.
2. D.M. Bernardi and M.W. Verbrugge, *J. Electrochem. Soc.* **139** (1992) 2477.
3. T.F. Fuller and J. Newman, *J. Electrochem. Soc.* **140** (1993) 1218.
4. T.V. Nguyen and R.E. White, *J. Electrochem. Soc.* **140** (1993) 2178.
5. T.E. Springer, M.S. Wilson and S. Gottesfeld, *J. Electrochem. Soc.* **140** (1993) 3513.
6. J.C. Amphlett, R.M. Baumert, R.F. Mann, B.A. Peppley, P.R. Roberge and T.J. Harris, *J. Electrochem. Soc.* **142** (1995) 9.
7. D.S. Watkins, K.W. Dircks, D.G. Epp, R.D. Merritt and B.N. Gorbell, US Patent 5 200 278 (1993).
8. J.C. Amphlett, R.M. Baumert, R.F. Mann, B.A. Peppley, P.R. Roberge and T.J. Harris, *J. Electrochem. Soc.* **142** (1995) 1.
9. F. Barbir and T. Gomez, *Int. J. Hydrog. Energy* **22** (1997) 1027.
10. A.M. El-Gammal, *J. Eng. Gas Turbines & Power* **113** (1991) 112.
11. J. Paduano, L. Valavani and A.H. Epstein, *J. Dynamic Syste., Meas., Control* **115** (1993) 694.
12. G. Heyen, K. Murphy, D. Marchio, P. Kalata, B. Kalitventzeff and E. Marechal, *Compute. Chem. Eng.* **18** (1994) 1071.
13. M. Cesar, M.M. Campos, P. Sergio and B. Rodrigues, *Oil & Gas J.*, **28**, (1988) 75.
14. J. Morè, B. Garbow, K. Hillstrom, 'Users's Guide for MINPACK-1', ANL-80-74 (1980), Argonne National Laboratory, 9700 S. Cass Avenue, Argonne, IL 60439.
15. R.H. Perry and D. Green (Eds) 'Perry's Chemical Engineers' Handbook' (McGraw-Hill, New York, 1984).
16. M. Muskat, 'Physical Principles of Oil Production' (McGraw-Hill, New York, 1949), Chapter 3.
17. T.V. Nguyen, *J. Electrochem. Soc.* **143** (1996) L103.
18. C. Cavalca, S.T. Homeyer and E. Walsworth, *US Patent 5 686 199* (1997).
19. D. Thirumalai and R.E. White, *J. Electrochem. Soc.* **144** (1997) 1717.
20. J.C. Amphlett, E.H. de Oliveira, R.F. Mann, P.R. Roberge, A. Rodrigues and J.P. Salvador, *J. Power Sources* **65** (1997) 173.